Published online 7 November 2011 *Nucleic Acids Research, 2012, Vol. 40, No. 4* ***1579–1595***
doi:10.1093/nar/gkr891

Direct evidence of nuclear Argonaute distribution during transcriptional silencing links the actin cytoskeleton to nuclear RNAi machinery in human cells

Chantelle L. Ahlenstiel[1,2,*], Heidi G. W. Lim[1,2], David A. Cooper[1,2], Takaomi Ishida[3], Anthony D. Kelleher[1,2] and Kazuo Suzuki[1]

[1]St Vincent's Centre for Applied Medical Research, Darlinghurst, [2]The Kirby Institute (formerly National Centre in HIV Epidemiology and Clinical Research), University of New South Wales, New South Wales, 2010, Australia and [3]Research Center for Asian Infectious Disease Institute of Medical Science University of Tokyo, Tokyo, Japan

Received November 30, 2010; Revised and Accepted October 3, 2011

ABSTRACT

Mammalian RNAi machinery facilitating transcriptional gene silencing (TGS) is the RNA-induced transcriptional gene silencing-like (RITS-like) complex, comprising of Argonaute (Ago) and small interfering RNA (siRNA) components. We have previously demonstrated promoter-targeted siRNA induce TGS in human immunodeficiency virus type-1 (HIV-1) and simian immunodeficiency virus (SIV), which profoundly suppresses retrovirus replication via heterochromatin formation and histone methylation. Here, we examine subcellular co-localization of Ago proteins with promoter-targeted siRNAs during TGS of SIV and HIV-1 infection. Analysis of retrovirus-infected cells revealed Ago1 co-localized with siRNA in the nucleus, while Ago2 co-localized with siRNA in the inner nuclear envelope. Mismatched and scrambled siRNAs were observed in the cytoplasm, indicating sequence specificity. This is the first report directly visualizing nuclear compartment distribution of Ago-associated siRNA and further reveals a novel nuclear trafficking mechanism for RITS-like components involving the actin cytoskeleton. These results establish a model for elucidating mammalian TGS and suggest a fundamental mechanism underlying nuclear delivery of RITS-like components.

INTRODUCTION

Argonaute proteins and small RNA duplexes are the primary components of effector complexes regulating transcriptional gene silencing (TGS) and post-transcriptional gene silencing (PTGS). Ago1 and sequence-specific siRNA are both essential components of the RNA-induced transcriptional silencing-like (RITS-like) complex, which directs siRNA-mediated TGS in mammalian cells (1,2). Ago1 also associates with RNA polymerase II (RNAPII) during siRNA-mediated TGS in humans (1). Both Ago1 and Ago2 can be found in the nucleus of human cells (3). We have previously shown sustained suppression of SIV and HIV-1 infections by siRNA-mediated TGS (4–7). This process is associated with modification of histone tails, recruitment of histone deacetylase 1 (HDAC1) and alteration of the chromatin structure within the retroviral LTR. The mechanism of siRNA-induced TGS is not well understood, particularly in mammalian cells, and there has been no direct visualization of RITS-like complex components in the nucleus.

For the RITS-like complex to function at the site of TGS, transport of the components from the cytoplasm into the nucleus is required. Actin is the major cytoskeleton component in the cytoplasm and among other cellular processes plays an important role in intracellular transport. Recent evidence has shown nuclear actin, actin-binding proteins (Abps) and actin-related proteins (Arps) are functionally important in the nucleus (8), with actin being required for transcription by RNAPII (9). Actin, Abps and Arps also functionally contribute to chromatin modifications. A link between actin and its related or binding proteins and siRNA-mediated TGS has not been previously shown.

Our study aimed to identify the subcellular localization of critical RITS-like complex components during siRNA-mediated TGS of SIV and HIV-1 infections, by examining confocal scanning immunofluorescent microscopy images of cells co-transfected with Ago1 or Ago2

*To whom correspondence should be addressed. Tel: +612 8382 4943; Fax: +612 8382 4967; Email: c.hood@amr.org.au

and promoter-targeted siRNAs. We observed that promoter-targeted siRNAs primarily co-localized with Ago1 in the nucleus of retrovirus-infected cells, while Ago2 was unexpectedly found to co-localize with promoter-targeted siRNAs primarily in the nuclear envelope of retrovirus-infected cells. We proceeded to investigate the mechanism trafficking our specific siRNAs to subcellular compartments during TGS of both retroviruses and revealed a novel association between F-actin and the nuclear compartment (comprised of both the nucleus and nuclear envelope) of retrovirus-infected cells during TGS. Furthermore, inhibition of actin filament polymerization by cytochalis in D reversed both F-actin and siRNA association with the nuclear compartment, which instead were observed in the cytoplasm of retrovirus-infected cells. Our findings show a distinct distribution of argonaute proteins in the nuclear compartment of retrovirus-infected cells during TGS and link the cytoskeleton with nuclear delivery of RITS-like complex components.

MATERIALS AND METHODS

Plasmid constructs and siRNAs

Expression plasmids encoding FLAG epitope-tagged human Ago1 (NM_012199) and Ago2 (NM_012154) were generated by cloning Ago1 or Ago2 into the pME-FLAG vector, which was kindly provided by Takaomi Ishida (10), using unique XhoI and SpeI restriction enzyme sites. SIV promoter-targeted siRNAs: si2A (5′-CCGCAAGAGGCCTTCTTA-3′) (4) and si2A-scrambled (5′-TAAAGCCTCAAACCCCGGTGT-3′) and SIV Gag-targeted siRNA: siGag (5′-GGATGTACAGACAACAGAA-3′) (4) were labeled on the 3′ end of the sense and antisense strands with AlexaFluor555. HIV-1 promoter-targeted siRNAs: siPromA (5′-GGGACTTTCCGCTGGGGACTT-3′) (5), siPromA-M2 (5′-GGGACTTTAAGCTGGGGACTT-3′) and siPromA-scrambled (5′-AAC-AGGCACACGTCCCAGCGT-3′) were labeled on the 3′ end of the antisense strand with AlexaFluor555 (Invitrogen). All AlexaFluor555-labeled siRNAs were 85–90% pure as determined by mass spectrometry analysis.

Cell culture

Media and reagents for cell culture were purchased from Gibco. MAGIC-5 and HeLa T4+ cells were grown in Dulbecco's modified Eagle's medium (DMEM) containing 10% fetal calf serum, 5 U/ml penicillin and 50 μg/ml streptomycin (supplemented DMEM) and incubated at 37°C in a humidified incubator with 5% CO_2.

Antibodies and fluorescent probes

Mouse monoclonal antibody against FLAG tagged epitope was used at 1:1000 dilution (Sigma, clone-M2 F1804). Rabbit monoclonal antibody directed against Lamin B was used at 1:500 dilution (Abcam). Normal mouse serum and normal rabbit serum antibody controls were used at 1:1000 and 1:500 dilutions, respectively (Invitrogen). AlexaFluor647-conjugated goat anti-mouse secondary antibody (Invitrogen) and AlexaFluor488-conjugated goat anti-rabbit secondary antibody (Invitrogen) were used at 1:200 dilution. AlexaFlour647-conjugated Phalloidin (AF647-Phalloidin) was used at 1:1000 dilution (Invitrogen). All antibody dilutions were made in a 10% normal goat serum (Invitrogen) and PBS diluent. The nuclear counterstain 4′,6-diamidino-2-phenylindole (DAPI) (Invitrogen) was used at 1:1000 dilution in PBS.

Retrovirus infections

For experiments using SIV-infected cells, 5×10^5 MAGIC-5 cells seeded into SlideFlasks (Nunc) in supplemented DMEM and following incubation for 16 h at 37°C in a humidified incubator with 5% CO_2 cells were inoculated with 1.5×10^7 RNA copies of SIVmac251. Cells were infected with SIV for 24 h prior to RNAi studies. In experiments using HIV-1_{SF162} infected cells, HIV-1_{SF162} was expanded using HUT78 cells, then HeLa T4+ cells were inoculated with 1×10^4 RNA copies and incubated for 9 days. Following this time, 5×10^5 infected HeLa T4+ cells were seeded into SlideFlasks in supplemented DMEM and following incubation for 16 h at 37°C in a humidified incubator with 5% CO_2 were used in RNAi studies. The HIV-1_{LAV} strain used was from a stably infected HeLa cell line, where greater than 90% of cells express the HIV-1 envelope protein, gp120 (11). Cells (5×10^5) were seeded into SlideFlasks in supplemented DMEM and following incubation for 16 h at 37°C in a humidified incubator with 5% CO_2 cells were used for RNAi studies.

RNA interference studies

Cells were transiently co-transfected with the expression plasmids and siRNAs described above using Lipofectamine2000 (Invitrogen) as per the manufacturer's instructions. Briefly, 5×10^5 cells in supplemented DMEM were seeded into SlideFlasks (Nunc) and incubated for 16 h at 37°C in a humidified incubator with 5% CO_2. Cells were co-transfected with 1 μg Ago1, Ago2 or empty vector plasmids and 0.64 nM siRNA using Lipofectamine2000 in OptiMEM medium (Invitrogen). Supplemented DMEM was added 4 h post-transfection and cells were processed 24 h later for immunofluorescence staining and supernatants were harvested to perform the reverse transcriptase (RT) assay measuring virus replication.

Drug treatment with cytochalisin D

Directly preceding co-transfection with FLAG-tagged constructs and siRNAs, mock-, SIV and HIV-1 infected cells were pre-treated for 1 h with cytochalisin D (cytD) (Sigma) at 1 μg/ml in 0.1% dimethyl sulfoxide (DMSO)/PBS. Parallel untreated cultures were exposed to 0.1% DMSO. Directly following the transfection process, cytD (1 μg/ml) was added to cells in OptiMEM medium. Supplemented DMEM was added 4 h post-transfection with 1 μg/ml cytD and cells were processed 24 h later for immunofluorescence staining.

Confocal immunofluorescent microscopy

Immunofluorescence microscopy was performed with MAGIC-5 and HeLa cells grown on SlideFlasks (Nunc). The cells were transiently co-transfected with Ago1 or Ago2 and promoter-targeted or control siRNAs as described above. After 24 h cells were washed in PBS and fixed in 4% formaldehyde (Sigma) for 10 min at RT. Cells were washed again in PBS and permeabilized with 0.3% Triton X-100 (Sigma) for 10 min at RT. To reduce non-specific binding cells were blocked in 10% normal goat serum for 30 min at 37°C in a humidified chamber and washed in PBS. All subsequent incubation steps were performed at 37°C in a humidified chamber. Cells were incubated for 1 h with primary antibodies specific for the FLAG-tag epitope, Lamin B or in subsequent experiments AF647-Phalloidin, washed thrice in PBS and incubated for 30 min with appropriate secondary antibodies. Cells were washed thrice in PBS and incubated with DAPI for 10 min at RT. Slides were mounted with coverslips and Fluromount G (Electron Microscopy Services). Confocal images of fluorescently labeled cells were acquired with a Leica inverted confocal laser scanning microscope (Leica TCS SP2) using a high-resolution Leica 63×/1.4 NA Plan Apo oil immersion objective and a pinhole aperture setting of 1 Airy unit. The microscope was equipped with Ar and HeNe laser lines 488 nm detecting AlexaFluor488, 543 nm to detect AlexaFluor555 and 633 nm to detect AlexaFluor647 and UV diode for 405 nm DAPI detection. Due to the broad emission spectra of these dyes, the fluorescent signals were collected only from peak regions and acquired sequentially. Images (8 bit) were acquired at scan speed (8 s per 1024 × 1024 pixels) to minimize the noise, with approximately 15 optical plane slices at 0.2 µm spacing in the *z*-axis. Image processing and generation of Pearson's coefficient correlation (PCC) values were performed using ImageJ software, Version 1.42q (National Institutes of Health, USA) (12), by first subtracting the background and then applying the Co-localization Analysis Plugin on the total image area, as described by (13). At least five PCC values were generated for each experimental treatment, from at least five randomly selected fields. Each field of view contained up to 40 cells (magnification 63×). Results were obtained from three independent experiments and data are shown from a representative experiment.

RT assay

Productive viral infection was quantified by RT activity in culture supernatants using the method previously described (14).

Cytoplasmic and nuclear protein extraction

HeLa cells were infected with HIV-1_{SF162} and transfected with FLAG-tagged Ago1 and promoter-targeted siPromA not labeled with AlexaFluor dye, as described above. Two days following transfection cells were washed with ice cold PBS and harvested using a cell scraper. The nuclear extraction protocol used has been adapted to meet PC3 laboratory requirements (15). Cells were washed in hypotonic buffer (10 mM Tris–HCl, pH 8.0, 0.32 M sucrose, 20 mM $MgCl_2$, 0.1 mM EDTA, 10 mM DTT and complete ultra EDTA-free protease inhibitors (Roche) (15). Following centrifugation cells were washed and lysed in hypotonic buffer during a 45 min incubation on ice. Nuclei were isolated and purified by passing lysate through a p200 pipette tip 20 times, followed by passage through a p20 tip 20 times. Nuclei were sedimented by centrifugation at 3000*g* at 4°C for 5 min, the supernatant containing cytoplasmic fraction was collected and the nuclear pellet was resuspended in hypotonic buffer containing 0.5 M sucrose and sedimented by centrifugation at 3000*g* at 4°C for 5 min. Nuclear proteins were isolated in extraction buffer (400 mM NaCl, 20 mM HEPES, pH 7.9, 25% glycerol, 1.5 mM $MgCl_2$, 0.4 mM EDTA, 1 mM DTT and complete ultra EDTA-free protease inhibitors) for 30 min at 4°C (15). Insoluble nuclear residues were sedimented at 3000*g* at 4°C for 10 min and the supernatant was collected. Collected cytoplasmic and nuclear fractions were applied for immunoprecipitation (IP).

IP, SDS–PAGE and western blot analysis

Protein fractions were diluted in two volumes of PBS to decrease the salt concentration and samples were incubated with anti-FLAG M2 agarose affinity gel overnight at 4°C with rotation. Immunoprecipitates were washed four times with PBS supplemented with complete ultra EDTA-free protease inhibitors. Loading buffer without reducing agent (Invitrogen) was added and samples were boiled for 5 min, centrifuged and supernatant was loaded onto an Invitrogen NuPage 4–12% Bis-Tris gel and separated for 35 min at 200 V. Separated proteins were transferred onto a PVDF membrane for 90 min at 30 V, blocked in 2.5% skimmed milk/TBS and immunoblotted with mouse anti-β-actin (1:2500, Sigma, A5441 clone AC-15) or rabbit anti-Argonaute 1/2/3/4 polyclonal antibody (1:500, Thermo Scientific, PA1-41178) at room temperature for 1 h or mouse anti-FLAG M2 (1:3000, Sigma, clone M2 F1804) (16) at 37°C for 1 h. All dilutions were prepared in 2.5% skimmed milk/TBS. Prior to addition of secondary sheep anti-mouse HRP antibody (1:3000) immunoblots were washed in TBS/0.1% Triton X-100. Immunoblots were developed using Immuno-Star HRP chemiluminescent reagents as per manufacturer's instructions (Bio-Rad) and visualized using Quantity One chemiluminescence software.

Statistical analysis

RT values are given as mean and SEM and were tested for significance using a paired, two-tailed *t*-test. PCC values are given as the mean and SEM and statistical comparisons of PCC correlations were performed using the non-parametric Mann–Whitney test, since the data are unpaired, and with the low sample number ($n = 5$ or 6) no assumption can be made regarding normal Gaussian distribution. A P-value <0.05 was considered statistically significant. All analyses were performed using Graphpad Prism Version 5.0 a (Graphpad Software, San Diego, CA, USA).

RESULTS

si2A targeting the promoter region suppresses SIV replication

Based on our previous report of si2A potently suppressing SIV replication through targeted promoter binding, we used this siRNA and a scrambled siRNA control AlexaFluor555-labeled at the 3′-ends of both antisense and sense strands (Figure 1A), with FLAG-tagged Ago1 or Ago2 constructs to examine their subcellular localization during RNA-induced TGS of SIVmac251 infection. Based on known argonaute sequences and domains, comprising of the N-terminus, a Piwi-Argonaute-Zwille (PAZ) domain, a MID domain and C-terminal PIWI domain, along with recent crystallography studies reporting the 5′ phosphate of small RNAs bind argonaute proteins via a binding pocket in the MID domain (17), we predicted that fusing a FLAG-tag to the N-terminal of our argonaute constructs would not interfere with this interaction. To confirm this, we assessed the fluorophore-labeled siRNAs ability to suppress SIV replication in the presence of N-terminal FLAG-tagged Ago1 and observed greater than 7-fold suppression on Day 6 post-infection when compared to scrambled siRNA (si2A-Sc-AF555) or mock controls as measured by reverse transcriptase (RT) assay (Figure 1B). We also confirmed the functionality of the FLAG-tagged Ago1 compared to endogenous Ago proteins by performing RT assays on SIV-infected cells transfected with the labeled siRNAs alone. We found that cultures transfected with FLAG-tagged Ago1 and si2A-AF555 had a significant twofold greater decrease in RT activity ($P = 0.0005$) compared to cells transfected with si2A-AF555 alone, indicting the transfected FLAG-tagged Ago construct expresses functional protein that contributes substantially to the observed viral suppression in addition to that mediated by endogenous Ago proteins alone (Figure 1B). This confirmed our previous study showing unlabeled si2A mediates SIV suppression via TGS (4) and demonstrate the addition of a fluorophore to the siRNA 3′-end (si2A-AF555) did not perturb its ability to suppress SIV replication, nor did the N-terminal FLAG-tag interfere with this process.

Ago1 co-localizes with si2A in the nucleus of SIV-infected cells

Having established the fluorophore-labeled siRNAs and FLAG-tagged Ago constructs were functional, we proceeded to investigate the subcellular compartments in which RITS-like components localize during TGS. We used MAGIC-5 cells, which express the preferred SIVmac251 co-receptor, CCR5 (along with CD4 and CXCR4), and infected with SIV or mock-infected for 24 h, then co-transfected with FLAG-tagged Ago1 or empty vector and si2A-AF555 or si2A-Sc-AF555 for a further 24 h. Following immunofluorescent staining, the cells were analyzed by confocal laser scanning microscopy. We observed si2A-AF555 and Ago1 localized predominantly to the cytoplasm of mock-infected cells, with some co-localization (Figure 2A). In stark contrast, si2A-AF555 and Ago1 were observed to co-localize in the nuclear compartment of SIV-infected cells (Figure 2B). Mock- and SIV-infected cells co-transfected with si2A-Sc-AF555 (Figure 2C) and Ago1 or empty vector controls showed only cytoplasmic staining and some low level co-localization. As expected the PTGS inducing Gag-specific siRNA, siGag-AF555, was observed in the cytoplasm, but not the nucleus, of both mock- and SIV-infected cells (Supplementary Figure S1A–B). The observations of Ago1:si2A and Ago1:siGag co-localizing, respectively, in the nucleus and cytoplasm of SIV-infected cells is consistent with TGS occurring in the nucleus and PTGS in the cytoplasm. Consistent with a previous study, we also observed larger siRNA aggregates compared to Ago protein staining patterns (18). No nuclear envelope co-localization with LaminB was observed for Ago1 or siRNAs in mock- or SIV-infected cultures. Image analysis revealed a significant co-localization between si2A-AF555 or Ago1 and the nucleus of SIV-infected

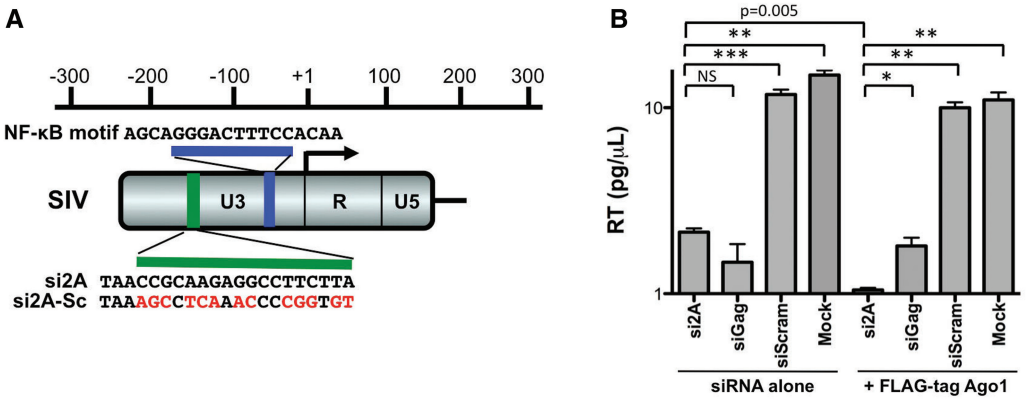

Figure 1. siRNA targeting the promoter region of SIVmac251 inhibits viral replication in MAGIC-5 cells. (**A**) 5′LTR sequence of SIVmac251 targeted by siRNAs; si2A and si2A-Scrambled control (si2A-Sc) are shown under the green bar at −164 bp. The NF-κB binding motif is shown above the blue bar at −49 bp. Nucleotide numbering is relative to the transcription start site. (**B**) The viral reverse transcriptase activity in culture supernatant, measured 6 days after virus infection of MAGIC-5 cells and transfection with FLAG-tagged Ago1 or without FLAG-tagged Ago1- and SIV-specific siRNAs; si2A and siGag, and specificity control, scrambled siRNA (si2A-Sc) or Lipofectamine2000 alone (mock) $*P \leq 0.02$, $**P = 0.002$, $***$ $P = 0.008$; NS, not significant; RT, reverse transcriptase.

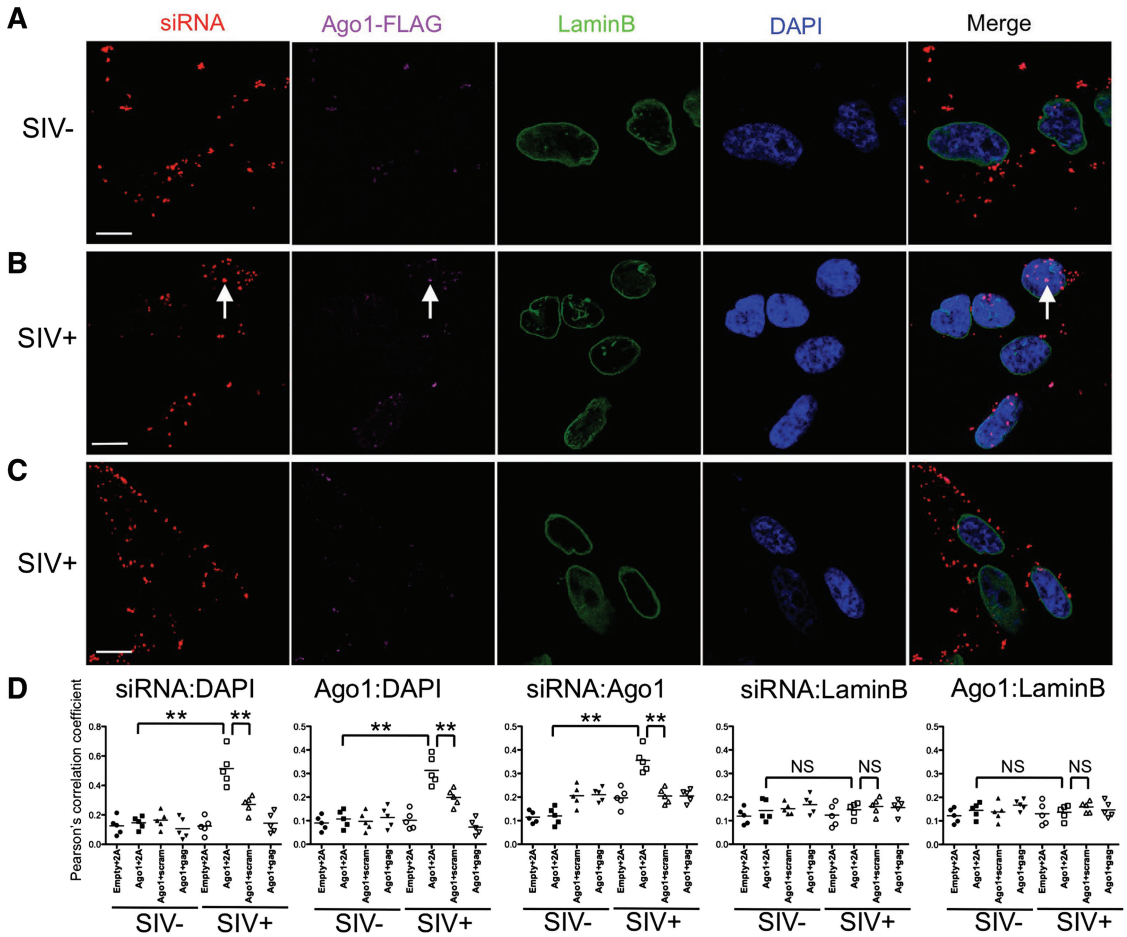

Figure 2. Immunofluorescent analysis of SIV promoter-targeted siRNA and Ago1 in MAGIC-5 cells. (**A**) Mock-infected cells co-transfected with Ago1 and si2A. (**B**) SIV-infected cells co-transfected with Ago1 and si2A. (**C**) SIV-infected cells co-transfected with Ago1 and scrambled siRNA. siRNAs (si2A and si2A-Sc) labeled with AF555 show red fluorescence, FLAG-tagged epitope representing Ago1 is labeled with AF647 (pseudocolored magenta), Lamin B labeled with AF488 (green fluorescence) indicates nuclear envelope and DAPI nuclear stain is pseudocolored blue. Arrows indicate nuclear localization in SIV-infected cells. Magnification 63×, scale bars indicate 5 μm. Images are representative of three experiments. (**D**) Pearson's correlation coefficient values are shown for siRNA and DAPI (left panel), Ago1 and DAPI (middle panel) and siRNA and Ago1 (right panel). $^{**}P = <0.008$.

cells as indicated by Pearson's correlation coefficient (PCC: 0.52 ± 0.05 and 0.31 ± 0.03, respectively) (mean ± SEM) compared to mock-infected cells (0.15 ± 0.02 and 0.11 ± 0.02, respectively) (both $P = 0.008$) and all other comparator cultures (Figure 2D). Although SIV-infected cells co-transfected with si2A-Sc-AF555 and Ago1 showed slightly increased PCC for nuclear co-localization (0.27 ± 0.03 and 0.19 ± 0.02, respectively), the mean values were still significantly lower compared to SIV-infected cells co-transfected with si2A-AF555 and Ago1 ($P = 0.008$). Importantly, a significant degree of co-localization was reported between si2A-AF555 and Ago1 in SIV-infected cells (0.36 ± 0.02) compared to mock-infected cells (0.12 ± 0.04) ($P = 0.002$). There were no significant correlations for siRNAs and Ago1 co-localization, nuclear localization (Figure 2D) or nuclear envelope localization (data not shown) observed in any other control cultures. These results clearly demonstrate Ago1 and the promoter-targeted si2A preferentially co-localize at the site of TGS in SIV-infected cells.

Ago2 co-localizes with si2A in the nuclear envelope of SIV-infected cells

To elucidate the subcellular localization of Ago2 during TGS of SIV, we co-transfected MAGIC-5 cells with Ago2 and the same panel of fluorophore-labeled siRNAs as in the previous experiments. Confocal images revealed si2A-AF555 and Ago2 localized to the cytoplasm of mock-infected cells, with some co-localization (Figure 3A). Intriguingly, SIV-infected cells co-transfected with Ago2 and si2A-AF555 displayed distinct nuclear envelope (LaminB) co-localization (Figure 3B), whereas mock- or SIV-infected cells co-transfected with si2A-Sc-AF555 (Figure 3C) or siGag-AF555 and Ago2 or empty vector controls all showed cytoplasmic staining only, with some co-localization (data not shown). Again as expected, siGag-AF555 and Ago2 were observed in the cytoplasm of mock- and SIV-infected cells, with some co-localization (Supplementary Figure S1C–D). This observation is consistent with sequence-specific siRNA (in our case siGag) and Ago2 being key components of RISC

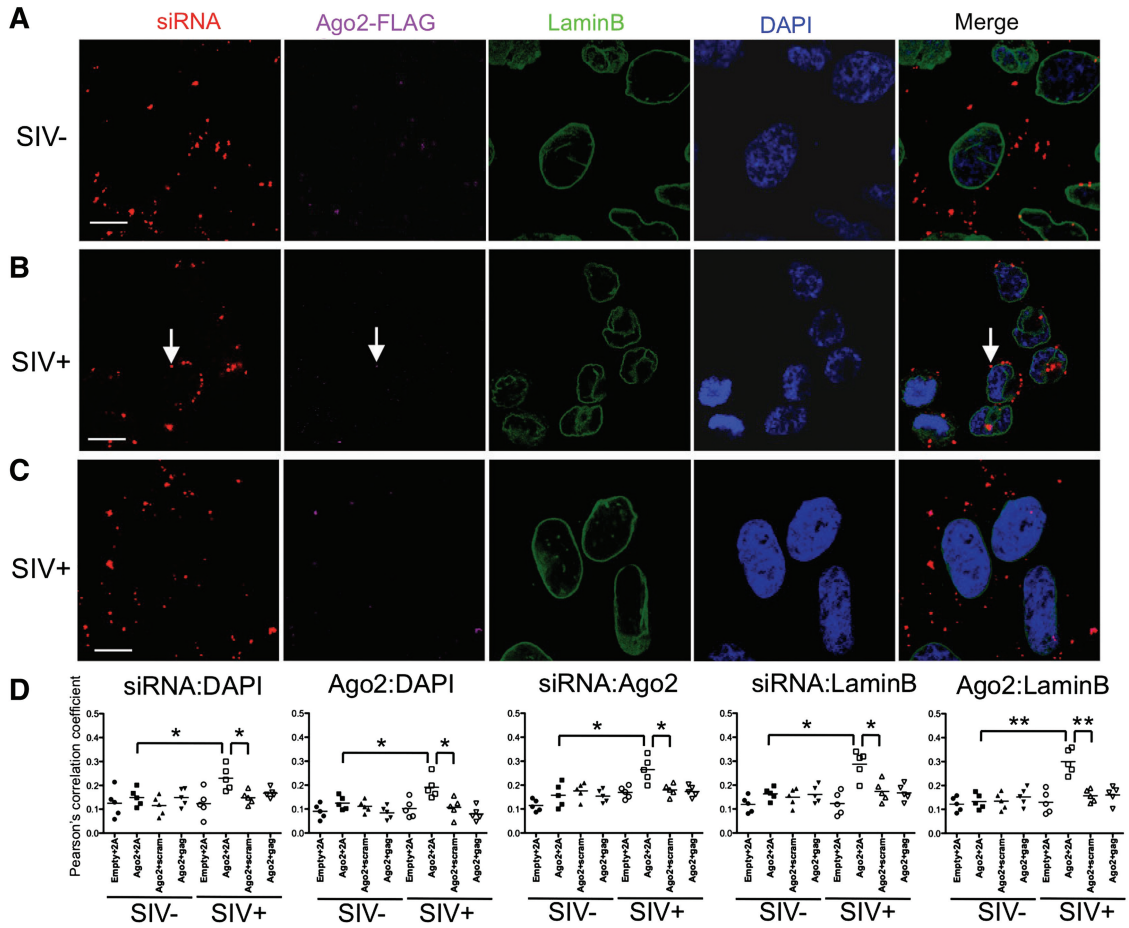

Figure 3. Immunofluorescent analysis of SIV promoter-targeted siRNA and Ago2 in MAGIC-5 cells. (**A**) Mock-infected cells co-transfected with Ago2 and si2A. (**B**) SIV-infected cells co-transfected with Ago2 and si2A. (**C**) SIV-infected cells co-transfected with Ago2 and scrambled siRNA. siRNAs (si2A and si2A-Sc) labeled with AF555 show red fluorescence, FLAG-tagged epitope representing Ago2 is labeled with AF647 (pseudocolored magenta), Lamin B labeled with AF488 (green fluorescence) indicates nuclear envelope and DAPI nuclear stain is pseudocolored blue. Arrows indicate nuclear localization in SIV-infected cells. Magnification x63, scale bars indicate 5 μm. Images are representative of three experiments. (**D**) Pearson's correlation coefficient values are shown for siRNA and DAPI (upper left panel), Ago2 and DAPI (upper middle panel), siRNA and Ago2 (upper right panel), siRNA and LaminB (lower left panel) and Ago2 and LaminB (lower right panel). $*P \leq 0.03$. $**P \leq 0.008$.

(19–21), leading to PTGS in the cytoplasm of SIV-infected cells. The PCC values confirmed a significant co-localization between the nuclear envelope of SIV-infected cells co-transfected with si2A-AF555 and Ago2 (0.29 ± 0.02 and 0.30 ± 0.02, respectively) compared to mock-infected cells (0.16 ± 0.01 and 0.13 ± 0.01, respectively) ($P = 0.02$ and 0.008, respectively) and all other cultures (Figure 3D). There was also a low degree of correlation between staining for either si2A-AF555 or Ago2 with the nucleus of SIV-infected cells (0.23 ± 0.02 and 0.19 ± 0.02, respectively) compared to mock-infected cells (0.14 ± 0.01 and 0.13 ± 0.01, respectively) (both $P = 0.03$). Importantly, si2A-AF555 and Ago2 showed a significant degree of co-localization in infected cells (0.27 ± 0.02) compared to mock-infected cells (0.15 ± 0.02) ($P = 0.02$). These data demonstrate that Ago2 and the promoter-targeted si2A, but not the control siRNAs, co-localize predominately within the nuclear envelope of SIV-infected cells.

siPromA suppresses HIV-1 virus replication

Based on our findings in SIV infection, we hypothesized that promoter-targeted siRNA and Ago1 and 2 proteins may co-localize similarly during RNA-induced TGS of HIV-1 infection. To test this hypothesis, we utilized two different HIV-1 subtype B strains, SF162 (a T cell line adapted CCR5-tropic virus) and LAV (a CXCR4-tropic virus) to assess whether the fluorophore-labeled siRNA were functional in suppressing HIV-1 subtype B virus infection. Our previous studies have described the siPromA sequence as a potent siRNA transcriptional suppressor of HIV-1, by interacting with the tandem NF-κB binding sites in the 5′LTR (5). We labeled this siRNA (siPromA), a two base pair mismatch siRNA (siPromA-M2) and a scrambled siRNA control (siPromA-Sc) with AF555 only on the antisense strand 3′ end and assessed whether virus suppression was disrupted by the addition of a 3′ fluorophore in the presence of FLAG-tagged Ago1

(Figure 4A). We observed >50-fold reduction in replication of HIV-1_{SF162} on Day 5 post-transfection when compared to scrambled and mismatched siRNAs or mock controls as measured by RT assay (Figure 4B). As above we reconfirmed the functionality of the FLAG-tagged Ago1 as well as FLAG-tagged Ago2 compared to endogenous Ago proteins by performing RT assays on HIV-1_{SF162} infected cells transfected with HIV-1 specific labeled siRNAs alone. Again, we found that cultures transfected with FLAG-tagged Ago1 and siPromA-AF555 or FLAG-tagged Ago2 and siPromA-AF555 had a significant 1.9-fold and 2.2-fold greater decrease in RT activity ($P = 0.03$ and 0.04, respectively) compared to cells transfected with siPromAA-AF555 alone, indicting the expression of FLAG-tagged Ago proteins is functional and contributes to a greater viral suppression than endogenous Ago proteins alone (Figure 4B). We also showed greater than 2-fold reduction in HIV-1_{LAV} replication on day 5 post-transfection with both labeled siRNAs and FLAG-tagged Ago1, compared to the scrambled and mismatched siRNAs or mock controls (Supplementary Figure S2A). These findings confirm our previous data showing unlabeled siPromA mediates HIV-1 suppression via TGS (5) and reiterates our SIV data by demonstrating the addition of a fluorophore to the 3′ siRNA end does not disrupt any interaction with the HIV-1 promoter region. This process appears to be highly specific as there was no impact on production of either virus strain mediated by the variant M2 siRNA, which only varies from the promA siRNA sequence by 2 bp, or the scrambled siRNA and confirms published specificity data using these siRNAs (16). These results show the antisense fluorophore-labeled siPromA successfully and specifically suppressed HIV-1 replication of both subtype B strains, SF162 and LAV.

Ago1 co-localizes with the antisense strand of siPromA in the nucleus of HIV-1 infected cells

To elucidate the subcellular localization of Ago1 and the promoter-targeted siPromA during TGS of HIV-1 infection, we used HIV-1_{SF162} or HIV-1_{LAV} infected and mock-infected HeLa T4+ cells co-transfected with FLAG-tagged Ago1 or empty vector and antisense strand AF555-labeled siPromA, along with siPromA-M2 or siPromA-Sc as controls. Following immunofluorescent staining, cells were analyzed by confocal laser scanning microscopy and both HIV-1 subtype B strain-infected cells displayed a similar Ago1:siRNA co-localization pattern to that observed in SIV-infected cells. Ago1 and antisense siPromA-AF555 localized to the cytoplasmic compartment of mock-infected cells, with some co-localization (Figure 5A, Supplementary Figure S2B), while Ago1 and antisense siPromA-AF555 predominantly co-localized in the nucleus of both HIV-1_{SF162} (Figure 5B) and HIV-1_{LAV} infected cells (Supplementary Figure S2C). In contrast, mock-, HIV-1_{SF162} (Figure 5C) and HIV-1_{LAV} infected cells (Supplementary Figure S2D) co-transfected with siPromA-Sc-AF555 and Ago1 (or empty vector, data not shown) displayed cytoplasmic staining and some co-localization. Similarly, mock- and all HIV-1 infected cells co-transfected with siPromA-M2-AF555 and Ago1 (or empty vector, data not shown) also revealed only cytoplasmic staining with some co-localization. Our observations of Ago1 and antisense siPromA predominantly co-localizing in the nucleus of HIV-1 infected cells are consistent with the nuclear TGS pathway and support our findings in SIV-infected cultures. PCC values generated by confocal image analysis showed a significant correlation between antisense siPromA-AF555 or Ago1 in the nucleus of HIV-1_{SF162} infected cells (0.36 ± 0.02 and 0.40 ± 0.02, respectively) compared to mock-infected cells (0.16 ± 0.02 and 0.15 ± 0.02, respectively) (both $P = 0.002$) and all other cultures (Figure 5D), with a similar correlation reported in the nucleus of HIV-1_{LAV} infected cells (Supplementary Figure S2E). No significant correlations for nuclear co-localization were reported in any mock-infected cells or HIV-1 infected cells co-transfected with siRNA controls; siPromA-Sc-AF555 and siPromA-M2-AF555, or empty vector. Once again, the promoter-targeted siRNA, siPromA and Ago1

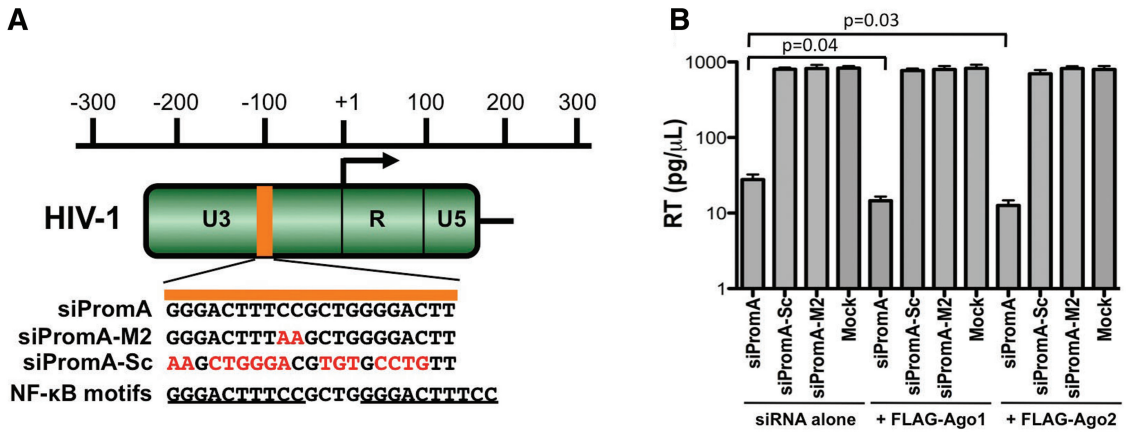

Figure 4. siRNA targeting the promoter region of HIV-1 inhibits viral replication in HeLa T4+ cells. (**A**) 5′LTR sequence of HIV_{SF162} and HIV_{LAV} targeted by siRNAs; siPromA, siPromA-Sc and siPromA-M2 control are highlighted. Nucleotide numbering is relative to the transcription start site. (**B**) Viral reverse transcriptase activity in culture supernatant, measured 5 days after infection of HeLa T4+ cells and transfection with siRNA alone, FLAG-tagged Ago1 or Ago2 and HIV specific siRNA; siPromA and specificity controls; siPromA-Sc and siPromA-M2 or Lipofectamine2000 alone (mock) $*P = < 0.02$, $**P = 0.002$, $***P = 0.008$.

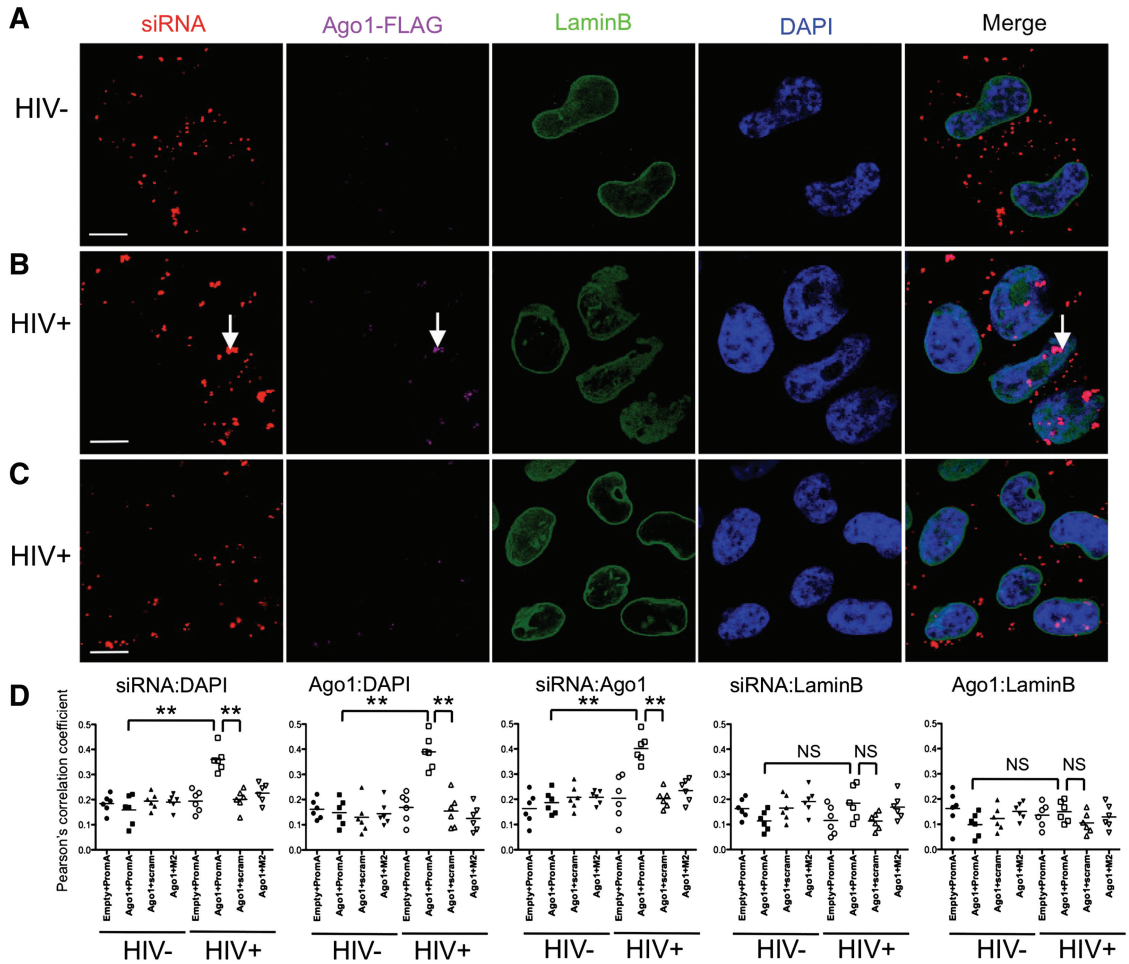

Figure 5. Immunofluorescent analysis of HIV-1 promoter-targeted siRNA and Ago1 in HeLa cells. (**A**) Mock-infected cells co-transfected with Ago1 and siPromA. (**B**) HIV_{SF162}-infected cells co-transfected with Ago1 and siPromA. (C) HIV_{SF162}-infected cells co-transfected with Ago1 and scrambled siRNA. siRNAs (siPromA and siPromA-Sc) labeled with AF555 show red fluorescence, FLAG-tagged epitope representing Ago1 is labeled with AF647 (pseudocolored magenta), Lamin B labeled with AF488 (green fluorescence) indicates nuclear envelope and DAPI nuclear stain is pseudocolored blue. Arrows indicate nuclear localization in HIV_{SF162}-infected cells. Magnification 63×, bars represent 5 μm. Images are representative of three experiments. (**D**) Pearson's correlation coefficient values are shown for siPromA and DAPI (left panel), Ago1 and DAPI (middle panel) and siPromA and Ago1 (right panel). $^{**}P = 0.002$.

showed a significant degree of co-localization in HIV-1_{SF162} infected cells (0.40 ± 0.02) compared to mock-infected cells (0.18 ± 0.02) ($P = 0.002$). These results clearly demonstrate that Ago1 co-localizes with the antisense strand of promoter-targeted siPromA in the nucleus of cells infected with either HIV-1_{SF162} or HIV-1_{LAV} strains.

Ago2 co-localizes with the antisense strand of siPromA in the nuclear envelope of HIV-1 infected cells

We also examined the subcellular compartmentalization of Ago2 and siPromA during TGS of HIV-1 infection, using HIV-1_{SF162} or HIV-1_{LAV} infected and mock-infected HeLa T4+ cells, co-transfected with Ago2 or empty vector and our panel of antisense strand fluorophore-labeled siRNAs. Confocal images again revealed cells infected with either HIV-1 subtype B strain showed the same intriguing Ago2:siRNA co-localization pattern as seen in SIV-infected cells. While mock-infected cultures displayed Ago2 and siPromA-AF555 localized to the cytoplasmic compartment, with some co-localization observed (Figure 6A), HIV-1_{SF162} (Figure 6B) and HIV-1_{LAV} infected cells (Supplementary Figure S3B) showed distinct nuclear envelope membrane co-localization of Ago2 and antisense strand siPromA-AF555. Mock- or HIV-1_{SF162} (Figure 6C) and HIV-1_{LAV} infected cells (Supplementary Figure S3C) co-transfected with siPromA-Sc-AF555 and Ago2 showed predominantly cytoplasmic staining, with some co-localization. Similarly, mock- and both HIV-1 subtype B strain infected cells co-transfected with siPromA-M2-AF555 and Ago2 (or empty vector, data not shown) also revealed predominantly cytoplasmic staining with some co-localization. ImageJ analysis showed a significant correlation between siPromA or Ago2 and nuclear envelope staining in HIV-1_{SF162} infected cells (0.38 ± 0.02 and 0.40 ± 0.03, respectively) compared to mock-infected cells (0.11 ± 0.02 and 0.10 ± 0.02, respectively) (both $P = 0.002$) and all other cultures (Figure 6D), with a similar correlation reported in

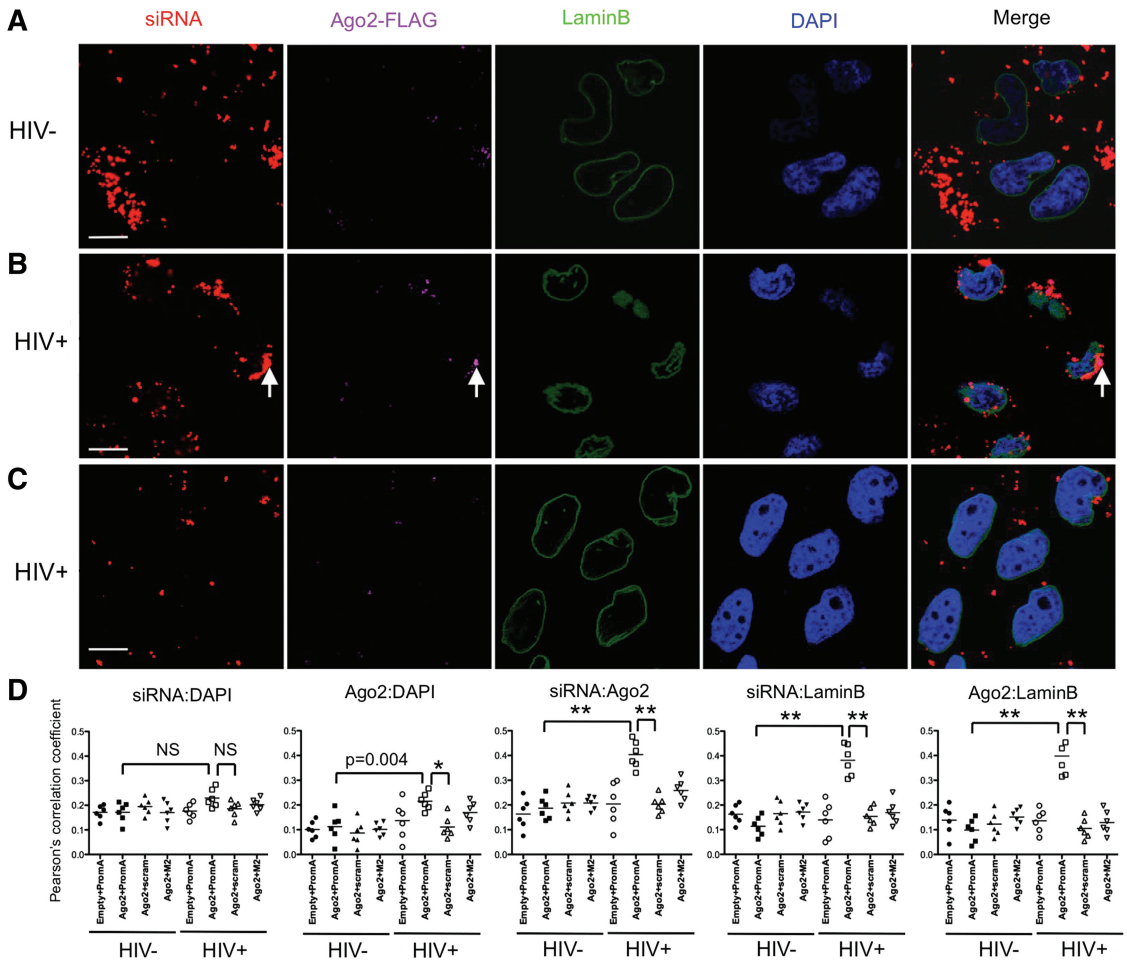

Figure 6. Immunofluorescent analysis of HIV-1 promoter-targeted siRNA and Ago2 in HeLa cells. (**A**) Mock-infected cells co-transfected with Ago2 and siPromA. (**B**) HIV_{SF162}-infected cells co-transfected with Ago2 and siPromA. (**C**) HIV_{SF162}-infected cells co-transfected with Ago2 and scrambled siRNA. siRNAs (siPromA and siPromA-Sc) labeled with AF555 show red fluorescence, FLAG-tagged epitope representing Ago2 is labeled with AF647 (pseudocolored magenta), Lamin B labeled with AF488 (green fluorescence) indicates nuclear envelope and DAPI nuclear stain is pseudocolored blue. Arrows indicate nuclear localization in HIV_{SF162}-infected cells. Magnification 63×, bars represent 5 μm. Images are representative of three experiments. (**D**) Pearson's correlation coefficient values are shown for siPromA and DAPI (upper left panel), Ago2 and DAPI (upper middle panel), siPromA and Ago2 (upper-right panel), siPromA and LaminB (lower left panel) and Ago2 and LaminB (lower right panel). NS, not significant. $*P = 0.01$, $**P = 0.002$.

the nuclear envelope of HIV-1_{LAV} infected cells (Supplementary Figure S3D). No significant correlations were reported in mock-infected cells or HIV-1 infected cells co-transfected with Ago2 or empty vector and siRNA controls; siPromA-Sc-AF555 and siPromA-M2-AF555. There was also no significant correlation between siPromA-AF555 staining and nuclear staining of HIV-1 infected cells. Ago2 showed some co-localization with the nucleus in HIV-infected cells compared to mock-infected cells ($P = 0.01$), although this correlation was due to overlap between the nucleus and the nuclear envelope and was no longer significant when compared to empty vector or siPromA-M2 transfected controls in infected cells. These results clearly demonstrate that Ago2 and the antisense strand of siPromA co-localize predominately within the nuclear envelope of cells infected with HIV-1_{SF162} or HIV-1_{LAV} subtype B strains.

Cytoplasmic actin filaments translocate to the nuclear compartment of retrovirus-infected cells during TGS

The distinct subcellular co-localization patterns of Ago1 and Ago2 with our promoter-targeted siRNAs during TGS of retroviral infections led us to investigate the mechanism trafficking RITS-like complex components to specific subcellular compartments. Since actin and Arps are known to be functional in chromatin-modifying complexes and play a role in intracellular transport, including actin-mediated entry of HIV into the nucleus (22), we hypothesized that the cytoskeleton, specifically its major actin component, was involved in delivering RITS-like complex components to their distinct subcellular sites. We investigated this using the same infection and co-transfection model as described in previous experiments, using SIV or HIV-1_{SF162} infected cells that were then co-transfected with the appropriate panels of

fluorophore-labeled siRNAs and Ago1 or empty vector for 24 h. We then immunofluorescently stained cellular actin filaments with Phalloidin-AF647, a mushroom-derived toxin specifically detecting actin polymers (F-actin), but not actin monomers (G-actin) (23). Since Phalloidin was labeled with the same fluorophore as our secondary antibody detecting FLAG-tagged Ago, we did not stain for Ago1 in this experiment and maintained the use of our established 4-color confocal imaging panel. We observed mock-infected cells co-transfected with si2A-AF555 (Supplementary Figure S4A) or siPromA-AF555 (Figure 7A) possessed normal cytoskeleton distribution, with F-actin fibers localized at the cell periphery and throughout the cytoplasm. Surprisingly, in SIV- (Supplementary Figure S4B) and HIV-1_{SF162} (Figure 7B) infected cells co-transfected with si2A-AF555 or siPromA-AF555, respectively, there was F-actin rearrangement and translocation of actin filaments to the nuclear compartment. In contrast, mock-, SIV- (Supplementary Figure S4C) and HIV-1_{SF162} (Figure 7C) infected cells co-transfected with scrambled siRNAs displayed cytoplasmic F-actin staining, as did mock- and retrovirus-infected cells co-transfected with siGag-AF555 or siPromA-M2-AF555 (data not shown). This illuminating result demonstrates siRNA-mediated TGS of retroviruses is associated with reorganization of the cytoskeleton, which may be involved in nuclear transport of siRNA in the RITS-like complex. Interestingly, while image analysis showed an expected significant correlation between si2A-AF555 or siPromA-AF555 and the nucleus of SIV- (Supplementary Figure S4D) or HIV-1_{SF162} (Figure 7D) infected cells (0.51 ± 0.05 and 0.31 ± 0.02, respectively) compared to mock-infected cells (0.15 ± 0.02 and 0.16 ± 0.02, respectively) ($P = 0.008$ and 0.002, respectively) and all other cultures, no significant co-localization was reported between si2A-AF555 or siPromA-AF555 and F-actin in the nucleus. This was despite low-level correlation between F-actin and the nucleus of SIV- and HIV-1_{SF162} infected cells (0.25 ± 0.02 and 0.22 ± 0.02, respectively) compared to mock-infected cells (0.09 ± 0.02

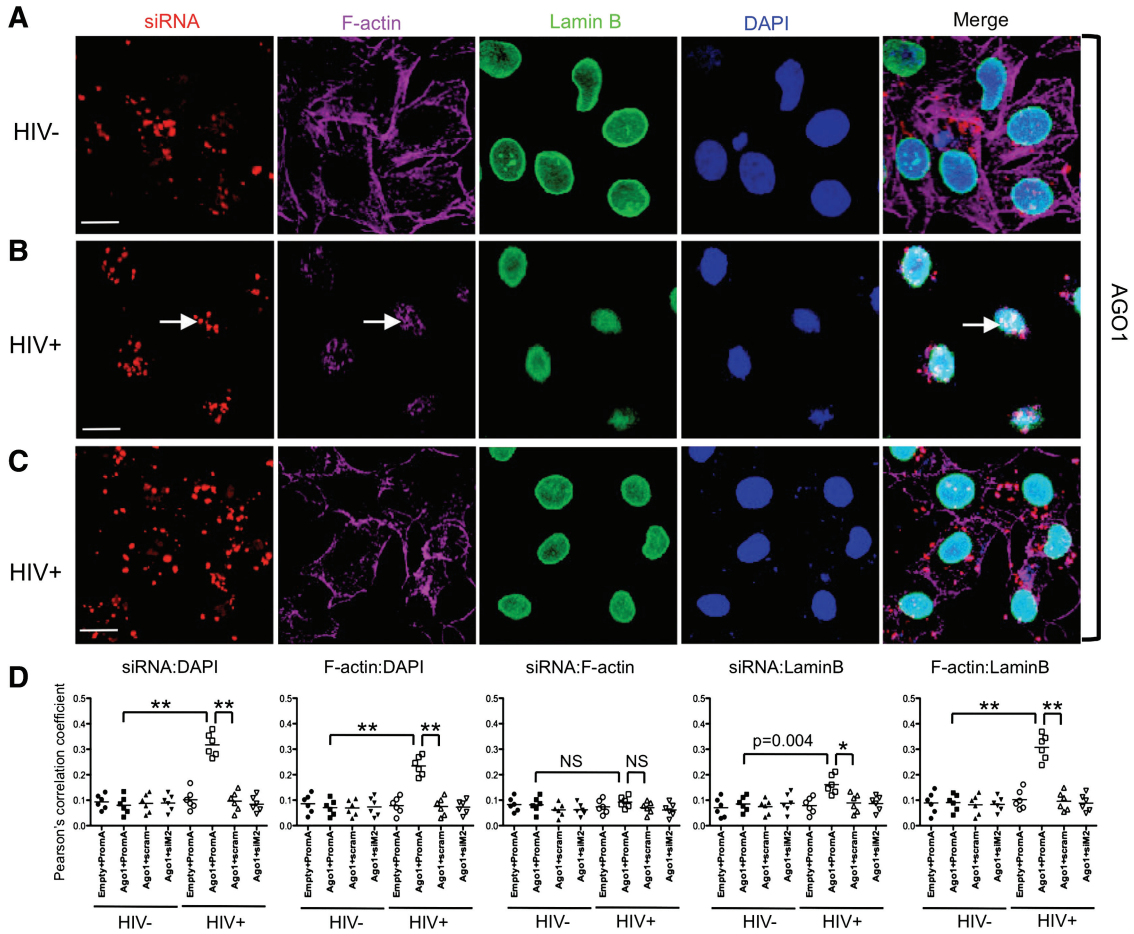

Figure 7. Immunofluorescent analysis of HIV-1 promoter-targeted siRNA and F-actin in HeLa cells. (**A**) Mock-infected cells co-transfected with Ago1 and siPromA. (**B**) HIV-infected cells co-transfected with Ago1 and siPromA. (**C**) HIV-infected cells co-transfected with Ago1 and scrambled siRNA. siRNAs (siPromA and siPromA-Sc) labeled with AF555 show red fluorescence, F-actin is labeled with phalloidin-AF647 (pseudocolored magenta), Lamin B labeled with AF488 (green fluorescence) indicates nuclear envelope and DAPI nuclear stain is pseudocolored blue. Arrows indicate nuclear localization in HIV-infected cells. Magnification 63×, bars represent 5 μm. Images are representative of three experiments. (**D**) Pearson's correlation coefficient values are shown for siPromA and DAPI (upper left panel), F-actin and DAPI (upper middle panel), siPromA and F-actin (upper right panel), siPromA and LaminB (lower-left panel) and F-actin and LaminB (lower right panel). NS, not significant. * $P = 0.02$, ** $P = 0.002$.

and 0.07 ± 0.01, respectively) (both $P = 0.002$). These results indicate a lack of co-localization in the nucleus between our promoter-targeted siRNAs and F-actin, even though both independently showed nuclear localization in retrovirus-infected cells. Even more interesting was our observation of a significant correlation between F-actin and the inner nuclear envelope membrane of SIV- and HIV-1_{SF162} infected cells co-transfected with si2A-AF555 or siPromA-AF555, respectively (0.35 ± 0.05 and 0.31 ± 0.02, respectively) compared to mock-infected cells (0.12 ± 0.02 and 0.09 ± 0.01, respectively) (both $P = 0.002$). No significant correlations for nuclear or nuclear envelope localization were reported in any mock-, SIV- or HIV-1 infected cells co-transfected with scrambled siRNA controls, siGag-AF555 or siPromA-M2-AF555. Our finding of cytoskeleton nuclear translocation during siRNA-mediated TGS in two retroviruses suggests actin filaments may be involved in nuclear transport of promoter-targeted siRNA in the RITS-like complex.

Actin filaments co-localize and biochemically associate with Ago1 and 2 in the nuclear compartment of HIV-1 infected cells during TGS

To determine whether F-actin and Ago1 interact spatially we performed the same infection and co-transfection model as described in previous experiments, using HIV-1_{SF162} infected cells that were then co-transfected with the appropriate panels of nonlabeled siRNAs and FLAG-tagged Ago1 or 2 or empty vector for 24 h. We then immunofluorescently stained cellular actin filaments with Phalloidin-AF647 and detected FLAG-tagged Ago1 or 2 with a secondary AF555 antibody to maintain the use of our established 4-color confocal imaging panel. We observed mock-infected cells co-transfected with siPromA-AF555 possessed normal cytoskeleton distribution, with F-actin fibers localized at the cell periphery and throughout the cytoplasm, and Ago1 or Ago2 also localized to the cytoplasm (Figure 8A and Supplementary Figure S5A, respectively). In contrast, HIV_{SF162} infected cultures showed F-actin and Ago1 clearly co-localized in the nucleus (Figure 8B), while F-actin and Ago2 co-localized to the nuclear envelope (Supplementary Figure S5B). Cultures transfected with siPromA-Sc-AF555 (Figure 8C and Supplementary Figure S7C) empty vector or mock-infected all showed clear cytoplasmic staining of both F-actin and Ago1 or 2. PCC values indicated a significant correlation between F-actin and Ago1 (Figure 8D) and F-actin and Ago2 (Supplementary Figure S5D) in infected cultures compared to mock-infected cultures transfected with siPromA-AF555 (0.29 ± 0.06 and 0.25 ± 0.04, respectively) (both $P = 0.002$). Interestingly, F-actin staining showed significant correlation with LaminB staining in both Ago1 or Ago2 transfected and siPromA-AF555 transfected cultures that were infected with HIV-1 compared to mock-infected cultures (0.25 ± 0.02 and 0.24 ± 0.02, respectively) (both $P = 0.002$). No significant correlations for nuclear or nuclear envelope localization were reported in any mock- or HIV-1 infected cells co-transfected with scrambled siRNA controls, siPromA-M2-AF555 or empty vector.

To definitively confirm the co-localization observed between F-actin and Ago1 occurs via a protein–protein association, we performed IP analysis of HIV-1_{SF162} infected cultures transfected with FLAG-tagged Ago1 or empty vector and unlabeled siPromA. We employed FLAG-M2 agarose affinity gel to pull-down FLAG-tagged Ago1 and associated proteins. Following immunoblotting using a β-actin specific antibody, we observed a 42 kDa band representative of β-actin in nuclear and cytoplasmic fractions of the IP samples of cultures transfected with FLAG-tagged Ago1, but not in cultures transfected with empty vector (Figure 8E, upper panel). We also immunoblotted for FLAG-tag using a FLAG-M2 specific antibody and showed FLAG-tag presence (~90 kDa band) in FLAG-tagged Ago1 transfected cultures (Figure 8E, lower panel). Further, we immunoblotted for Ago protein using an Ago-specific antibody and showed Ago protein (~90 kDa band) was present in all input samples, but only in the nuclear IP fraction of Ago1-transfected cultures (Figure 8E middle panel). Our findings clearly demonstrate both co-localization of F-actin and FLAG-tagged Ago1 or 2 and a protein interaction between F-actin and FLAG-tagged Ago1 during siRNA-mediated TGS, suggesting that actin filaments may be involved in nuclear transport of Ago1 in a RITS-like complex.

Actin filament depolymerization by cytochalisin D disrupts nuclear translocation of F-actin, promoter-targeted siRNA and Ago1 and 2

To confirm our findings of cytoskeleton involvement in nuclear transport of promoter-targeted siRNA, we pretreated mock-, SIV- or HIV_{SF162} infected cells with the actin depolymerising agent, cytochalisin D (cytD). The fungal toxin cytD inhibits actin polymerization by binding to the polymeric actin plus end and prevents addition of monomeric actin (24). Following cytD treatment, we transfected FLAG-tagged Ago1 and our panel of fluorophore-labeled siRNAs, and then immunofluorescently stained the cytoskeleton actin filaments with phalloidin-AF647 24 h later. Analysis by confocal laser scanning microscopy revealed that treatment with cytD disrupted nuclear trafficking, with no nuclear localization observed for F-actin or siRNAs in any cytD treated SIV- or HIV-1_{SF162} infected cultures. As shown in our previous experiment, cytD untreated SIV- (Supplementary Figure S6A) and HIV-1_{SF162} (Figure 9A) infected cells co-transfected with Ago1 and si2A-AF555 or siPromA-AF555, respectively, were associated with F-actin and promoter-targeted siRNA redistribution to the nuclear compartment. In stark contrast, when we pretreated SIV- (Supplementary Figure S6B) and HIV-1_{SF162} (Figure 9B) infected cells with cytD, followed by co-transfection with Ago1 and si2A-AF555 or siPromA-AF555, respectively, we observed disordered, punctate F-actin in the cytoplasm with less peripheral staining and cytoplasmic siRNA staining. Mock-, SIV- and HIV-1_{SF162} infected cells not treated with cytD and

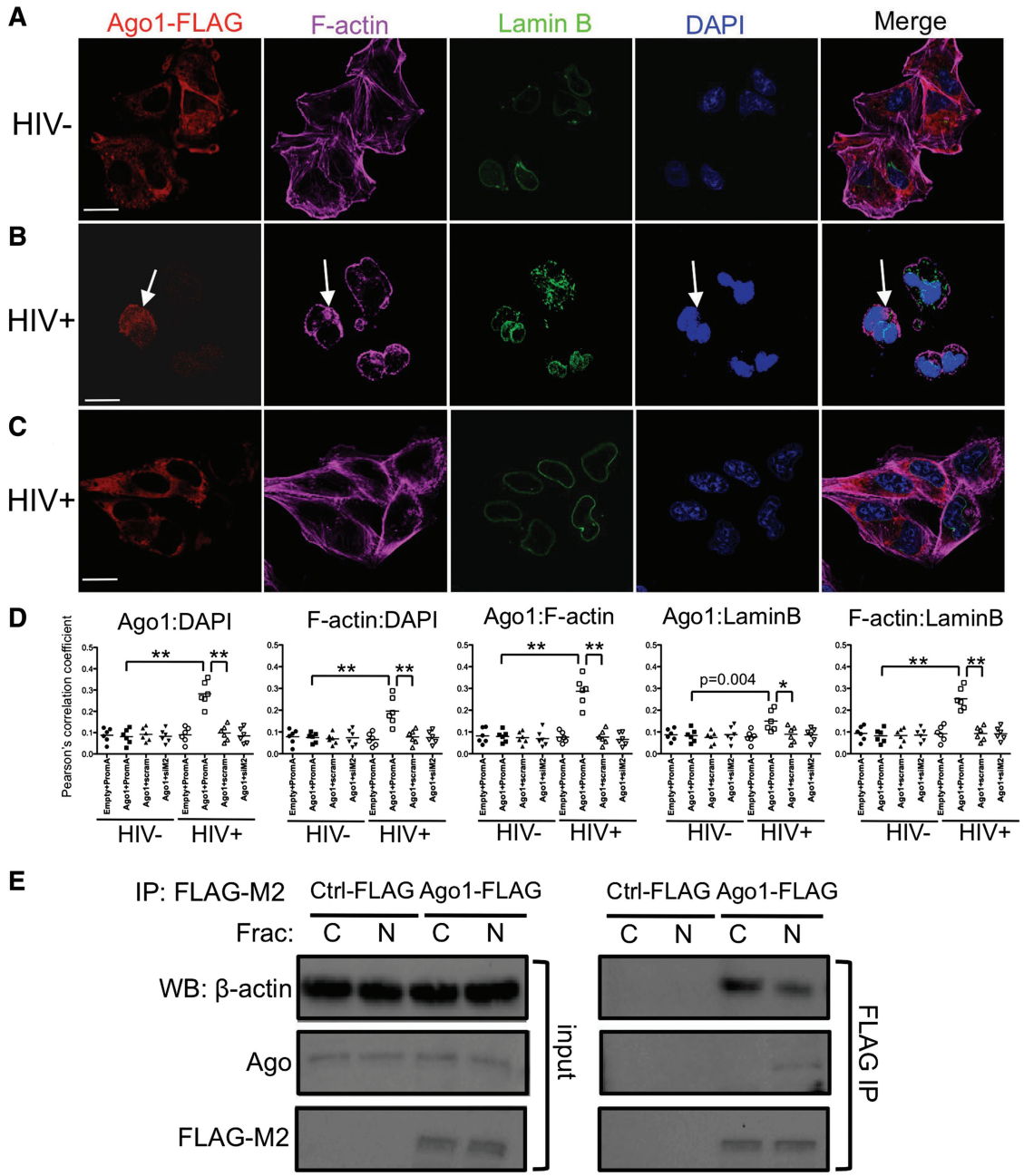

Figure 8. Immunofluorescent analysis of Ago1 and F-actin in HIV-1-infected HeLa cells. (**A**) Mock-infected cells co-transfected with Ago1 and unlabeled siPromA. (**B**) HIV-infected cells co-transfected with Ago1 and siPromA. (**C**) HIV-infected cells co-transfected with Ago1 and scrambled siRNA. Ago1 labeled with AF555 shows red fluorescence, F-actin is labeled with phalloidin-AF647 (pseudocolored magenta), Lamin B labeled with AF488 (green fluorescence) indicates nuclear envelope and DAPI nuclear stain is pseudocolored blue. Arrows indicate nuclear localization in HIV-infected cells. Magnification 63×, bars represent 5 μm. Images are representative of three experiments. (**D**) Pearson's correlation coefficient values are shown for Ago1 and DAPI (upper left panel), F-actin and DAPI (upper middle panel), Ago1 and F-actin (upper right panel), Ago1 and LaminB (lower left panel) and F-actin and LaminB (lower right panel). NS, not significant. $*P = 0.02$, $**P = 0.002$. (**E**) IP analysis of HIV-1 infected cells transfected with FLAG-tagged Ago1 or empty vector and siPromA. Cytoplasmic and nuclear fractions applied to IP are shown in the left panel (input) and proteins that immunoprecipitated with the FLAG-M2 agarose affinity gel are shown in the right panel (IP samples). Samples were probed by western blot with antibodies to β-actin (upper panel), Ago (middle panel) or FLAG-M2 (lower panel). WB, western blot; Frac, fraction; C, cytoplasmic; N, nuclear; Ctrl-FLAG, control empty vector.

co-transfected with Ago1 and scrambled siRNAs, siGag-AF555 or siPromA-M2-AF555 all showed normal cytoplasmic F-actin distribution and predominantly cytoplasmic siRNA localization. Similarly, mock-, SIV- and HIV-1_{SF162} infected cells that were treated with cytD, then co-transfected with Ago1 and scrambled siRNAs (Figure 9C and Supplementary Figure S6C), siGag-AF555 or siPromA-M2-AF555 also showed cytoplasmic siRNA localization, along with disordered and punctate cytoplasmic F-actin, with less cell periphery

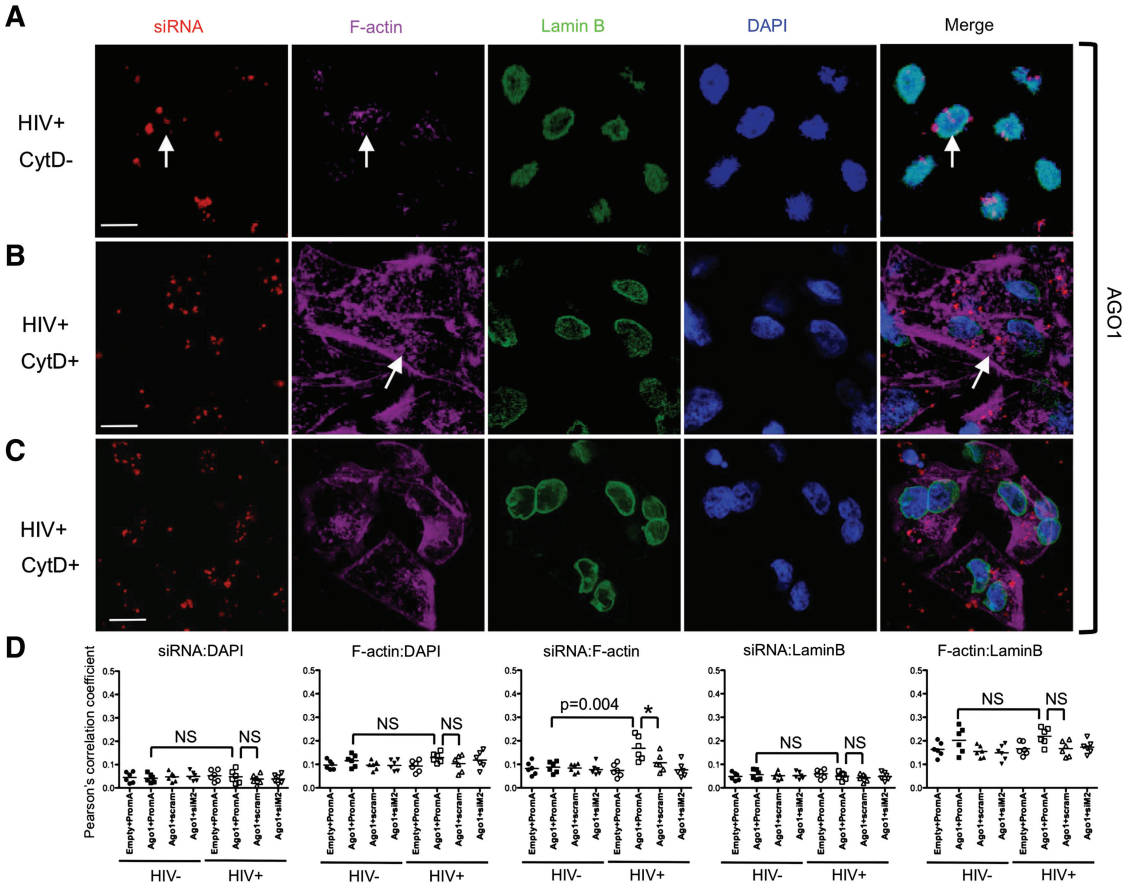

Figure 9. Immunofluorescent analysis of HIV-1 promoter-targeted siRNA and F-actin in cytochalisin D-treated HeLa cells. (**A**) HIV-1_{SF162} infected cells co-transfected with Ago1 and siPromA, not treated with cytochalisin D (CytD). (**B**) HIV-1_{SF162} infected cells co-transfected with Ago1 and siPromA, not treated with CytD. (**C**) HIV-1_{SF162} infected cells pre-treated with cytochalisinD and co-transfected with Ago1 and siPromA. siRNAs labeled with AF555 show red fluorescence, F-actin is labeled with phalloidin-AF647 (pseudocolored magenta), Lamin B labeled with AF488 (green fluorescence) indicates nuclear envelope and DAPI nuclear stain is pseudocolored blue. Arrows indicate nuclear localized F-actin staining in panel b and punctate cytoplasmic F-actin staining in (C). Magnification 63×, bars represent 5 μm. Images are representative of three experiments. (D) Pearson's correlation coefficient values for CytD treated cultures are shown for siRNA and DAPI (left panel), F-actin and DAPI (middle panel) and siRNA and F-actin (right panel). NS, not significant; $*P = 0.01$.

staining due to depolymerization by cytD. Importantly, image analysis showed no significant nuclear localization of F-actin or siRNAs in any of the cytD treated SIV- (Supplementary Figure S6D) or HIV-1_{SF162} (Figure 9D) infected cultures. An interesting finding we only observed in cytD cultures was a significant level of cytoplasmic co-localization between F-actin and si2A-AF555 or siPromA-AF555 in SIV- and HIV-1_{SF162} infected cells, respectively (0.19 ± 0.02 and 0.17 ± 0.02, respectively), compared to mock-infected cells (0.08 ± 0.01 and 0.09 ± 0.01, respectively) (both $P = 0.01$) and all other cultures (Figure 9D, Supplementary Figure S6D). This indicates F-actin and promoter-targeted siRNAs have the ability to be spatially related as shown by co-localization in the cytoplasm. We observed slightly higher PCC values quantifying co-localization between F-actin and the nuclear envelope in all cytD treated mock-, SIV- and HIV-1_{SF162} cultures compared to untreated cultures; however, this was an effect of F-actin depolymerization and was not significant when compared amongst all cytD-treated cultures.

We then investigated the effect of cytD treatment on the localization of F-actin and Ago1 and 2 using the same HIV-1 experimental model as above, but with unlabeled siRNA so we could stain FLAG-tagged constructs with AF555 secondary antibody and maintain our 4-color confocal staining panel. We observed consistent cytoplasmic staining of Ago1 and 2 and disordered, punctate F-actin staining in the cytoplasm of all cultures treated with cytD and transfected with siPromA, specificity controls or empty vector (Supplementary Figure S7A–D). Further, there were no significant correlations observed for any fluorescently stained markers (Ago1 and 2, F-actin, DAPI and LaminB) (Supplementary Figure S7E and F). Together these findings suggest polymeric actin filaments are involved in delivering promoter-targeted siRNAs and Ago1 and 2 to the nuclear compartment during TGS of retroviruses.

DISCUSSION

We investigated the mechanisms of siRNA-induced TGS during retrovirus infection by direct visualization of

critical components of RITS-like complex. We describe both distinct subcellular distribution of RITS-like complex components and a novel nuclear transport mechanism for RITS-like components mediated by the actin filament (F-actin) component of the cytoskeleton. Ago1 and promoter-targeted siRNAs were found preferentially in the nucleus of retrovirus-infected cells, while Ago2 and promoter-targeted siRNAs were found in the inner nuclear envelope of retrovirus-infected cells. The distinct nuclear compartmentalization of these RITS-like components was observed only in infected cultures, suggesting accumulation of RITS-like components in the nucleus of infected cells during TGS. The clear association between Ago1 and promoter-targeted siRNAs in the nucleus is consistent with the site of TGS being nuclear and supports previous studies suggesting Ago1 and siRNAs are RITS-like complex components (2,4). Our interesting finding that Ago2 co-localized with promoter-targeted siRNAs in the inner nuclear lamin membrane indicated the association alone between Ago2 and promoter-targeted siRNAs was not sufficient for nuclear transport. This may be due to Ago2 possibly requiring Ago1 for nuclear trafficking as part of the RITS-like complex. Our experiments, which separately expressed exogenous FLAG-tagged Ago1 or Ago2, but not both combined, may indicate the low endogenous levels of Ago1 are not adequate to facilitate nuclear transport of exogenous FLAG-tagged Ago2 protein. It is tempting to speculate that Ago2 could also be retained in the nuclear pore complex (NPC), further regulating traffic of protein complexes between the nucleus and cytoplasm (25); however, additional co-localization studies are required for confirmation.

This study demonstrated the distinct distribution of Ago:siRNAs using two different retroviruses; SIVmac251 and two different HIV-1 subtype B strains: CXCR4-tropic HIV-1_{SF162} and CCR5-tropic HIV-1_{LAV}. Observing the same phenomenon in all three retrovirus infection TGS models highlights that the findings are compelling. Moreover, it is important to appreciate that the si2A sequence, targeting a region well upstream of the SIV NF-κB binding motif, is quite different from the siPromA sequence, targeting the tandem NF-κB binding motifs in the HIV-1 5' LTR promoter region. To provide important specificity controls for our experiments, we showed that scrambled siRNAs and siPromA-M2, which varies from HIV-1 promoter-targeted siPromA by only two bp, had no effect on nuclear co-localization of RITS-like components and were instead found in the cytoplasm. We also confirmed the previously reported finding that the antisense siRNA strand participates in the formation of the RITS-like complex in human cells (26,27), as shown by our experiments using two different HIV-1 subtype B strains, where only the antisense strand of siPromA was labeled.

The distinct subcellular compartmentalization of Ago:siRNA led us to investigate the mechanism regulating nuclear transport of these RITS-like components. Studies in *S. pombe* have found RNAi machinery proteins and RNAi-associated P bodies are transported via cytoskeleton microtubule networks in the cytoplasm (28–30). A recent report further describes the microtubule-associated kinesin motor protein Cut7 regulates cytoplasmic RNAi effector complexes during PTGS, but not TGS (31). Our study focused on elucidating mechanisms of the TGS pathway and reports the novel finding of cytoskeleton polymeric actin being linked to transport of promoter-targeted siRNAs as part of RNAi machinery in the nucleus of mammalian cells. Although both promoter-targeted siRNAs and F-actin were found to localize to the nucleus of retrovirus-infected cells, there was no significant co-localization of these two molecules within the nucleus as quantified by PCC values. This indicates that while F-actin may play a role in nuclear trafficking of promoter-targeted siRNAs, it may not necessarily directly interact with siRNA:Ago1 in the nucleus during transcriptional suppression, although Ago1 was observed to directly associated with β-actin by immunoprecipiation. Furthermore, when we depolymerized actin using cytD treatment, we did find significant co-localization between F-actin and promoter-targeted siRNAs in the cytoplasm, demonstrating that they are spatially related in this compartment and could interact. Alternately, Abps are known to be involved in nucleocytoplasmic transport and may provide the bridging link between the long filamentous F-actin structure and promoter-targeted siRNAs. This may also account for the biochemical association observed between F-actin and Ago1, although the effect could also be a direct protein interaction but fine delineation of this requires further investigation. Abps proteins associate with actin to continuously regulate actin polymerization, cross-link actin filaments and move cargo along the filaments. The TGS pathway may utilize this association to load RITS-like complex components onto actin filaments in the cytoplasm, traffic them into the nuclear compartment, then disassociate from the actin filament once in the nucleus.

Cofilin, is one such Abp essential for chaperoning actin into the nucleus, as shown by an associated block in nuclear actin accumulation upon inhibiting cofilin (32). Another Abp of interest is the giant NUANCE (NUcleus and ActiN Connecting Element) protein, also termed Nesprin-2 Giant (33). This mammalian nesprin protein has an N-terminal region comprising of an α-actinin-type actin-binding domain, which facilitates the physical connection between the nucleus and actin cytoskeleton. Nesprins also interact with emerin in the inner nuclear membrane (34), where emerins have been shown to bind F-actin (35). Interestingly, Arps have also been found in the nucleus and physically interact with chromatin-modifying complexes, specifically Arp4 and 6, which co-localize with heterchromatin protein 1 (HP1) in *Drosophila* (36,37). The Arp BAF53 also associates with actin as part of the BAF chromatin-modifying complex in humans (38). Many proteins have also been identified to associate with Ago1 and Ago2 as part of the RNAi machinery. These include TBRC6B, MOV10, nuclear DNA helicase II (also termed RNA helicase A), Importin 8, Gemin3, Gemin4, HDAC-1 and EZH2 (1,5,39,40). Furthermore, nuclear DNA helicase II has been shown to bind F-actin in the nucleus of human cells (41). All of these proteins are further candidates worthy of

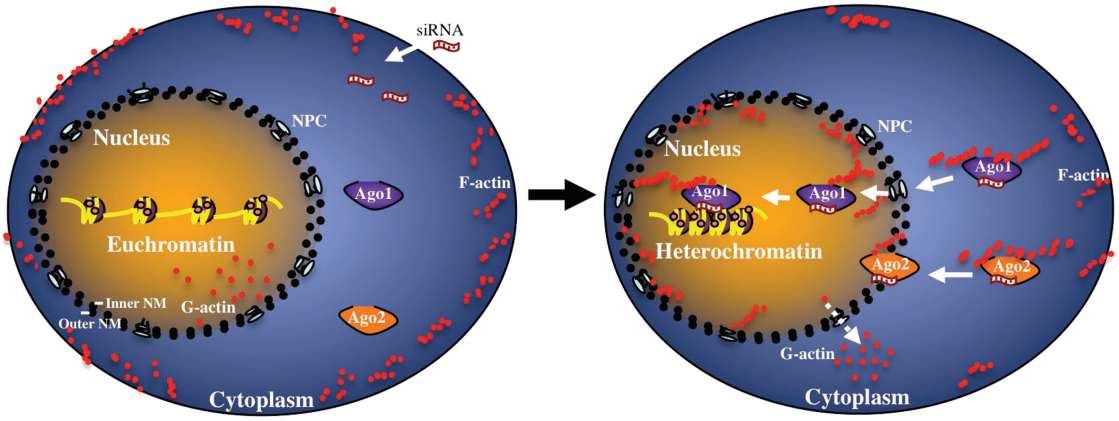

Figure 10. Model of the actin cytoskeleton role in nuclear trafficking of mammalian RITS-like complex components. Our results show that Ago1 and promoter-targeted siRNA co-localize in the nucleus of retrovirus-infected cells as part of the RITS-like complex during TGS, while Ago2 and promoter-targeted siRNAs co-localize in the inner nuclear envelope membrane (inner NM) of retrovirus-infected cells during TGS. Our findings suggest that nuclear delivery of RITS-like complex components, specifically promoter-targeted siRNAs associated with Ago1, involves the cytoskeleton actin filament (F-actin), probably via active transport through the nuclear pore complex (NPC). In response to F-actin translocating into the nucleus, we speculate that monomeric actin (G-actin) levels would increase in the cytoplasm. Shown on the left is a cell actively undergoing transcription, prior to transfected siRNAs associating with Ago protein/s. On the right is a cell undergoing TGS, where the siRNAs have associated with Ago protein/s and are trafficked into the nucleus with the involvement of the actin cytoskeleton.

investigation using our model to dissect the mechanisms of mammalian TGS.

Nuclear actin and myosin are also reported to regulate nucleo-cytoplasmic transport, possibly as NPC components (42). This nucleo-cytoplasmic transport is an ATP-dependent process and is inhibited by cytD treatment (42), suggesting that our observations of siRNA nuclear import inhibition during cytD treatment also indicates nuclear import of RITS-like components is an ATP-dependent process. Nuclear import of some Ago proteins also requires association with siRNAs, as demonstrated for the *C. elegans* Ago protein NRDE-3 (43). Moreover, in mice the Ago protein MIWI2 binds Piwi-associated (pi) RNAs and is localized to the nucleus (44). Another study shows the protozoan *Tetrahymena* Ago protein Twi1p associated with siRNA is transported into the nucleus via Giw1p (45). These studies suggest a mechanism that selectively transports only Ago proteins that are associated with siRNAs. Our findings support this selection mechanism, which would explain why we only observed co-localized FLAG-tagged Ago and siRNA in the nucleus of retrovirus-infected cells and not Ago or siRNA alone.

Our study shows a distinct subcellular distribution of Ago proteins and promoter-targeted siRNAs in the nuclear compartment of retrovirus-infected cells and directly links the actin cytoskeleton with nuclear delivery. We propose a model for the nuclear import of RITS-like components whereby F-actin translocation into the nuclear compartment, primarily the inner nuclear membrane, corresponds to nuclear delivery of promoter-targeted siRNAs, which then recruit other proteins to form the nuclear RITS-like complex (Figure 10). Although we have shown both co-localization and a direct biochemical interaction between F-actin and FLAG-tagged Ago1 protein in the nucleus of retrovirus-infected cells, it is important to understand that other factors may also interact with actin filaments in the cytoplasm to facilitate the mechanical delivery of promoter-targeted siRNAs and Ago proteins into the nuclear compartment. It is likely that other factors also contribute to nuclear transport and regulation of this process during TGS warrants further investigation. The findings of our study present direct visualization of siRNA, Ago1 and Ago2 in the mammalian TGS pathway. The study also provides valuable insight into the fundamental mechanism underlying nuclear trafficking of RITS-like complex components by the actin cytoskeleton, which may also be functional in lower eukaryotes.

SUPPLEMENTARY DATA

Supplementary Data are available at NAR Online: Supplementary Figures S1–S7.

ACKNOWLEDGEMENTS

SIVmac251 was obtained from National Institutes of Health AIDS Research (cat. nos. 160), Shinichi Oka and Masashi Tastumi (National Institute of Infectious Diseases and AIDS Clinical Center, International Medical Center of Japan, Tokyo, Japan) kindly provided the MAGIC-5 cells. We thank Tri Phan (Garvan Institute) for helpful discussions of our initial confocal microscopy experiments. The views expressed in this publication do not necessarily represent the position of the Australian Government. The Kirby Institute is affiliated with the Faculty of Medicine, University of New South Wales.

FUNDING

Australian Government Department of Health and Ageing (RM07292); National Health and Medical Research Council (455350 to A.K., 630571 for K.S. and

C.H.). Funding for open access charge: St Vincent's Centre for Applied Medical Research.

Conflict of interest statement. None declared.

REFERENCES

1. Kim,D.H., Villeneuve,L.M., Morris,K.V. and Rossi,J.J. (2006) Argonaute-1 directs siRNA-mediated transcriptional gene silencing in human cells. *Nat. Struct. Mol. Biol.*, **13**, 793–797.
2. Morris,K.V., Chan,S.W., Jacobsen,S.E. and Looney,D.J. (2004) Small interfering RNA-induced transcriptional gene silencing in human cells. *Science*, **305**, 1289–1292.
3. Robb,G.B., Brown,K.M., Khurana,J. and Rana,T.M. (2005) Specific and potent RNAi in the nucleus of human cells. *Nat. Struct. Mol. Biol.*, **12**, 133–137.
4. Lim,H.G., Suzuki,K., Cooper,D.A. and Kelleher,A.D. (2008) Promoter-targeted siRNAs induce gene silencing of simian immunodeficiency virus (SIV) infection in vitro. *Mol. Ther.*, **16**, 565–570.
5. Suzuki,K., Juelich,T., Lim,H., Ishida,T., Watanebe,T., Cooper,D.A., Rao,S. and Kelleher,A.D. (2008) Closed chromatin architecture is induced by an RNA duplex targeting the HIV-1 promoter region. *J. Biol. Chem.*, **283**, 23353–23363.
6. Suzuki,K., Shijuuku,T., Fukamachi,T., Zaunders,J., Guillemin,G., Cooper,D. and Kelleher,A. (2005) Prolonged transcriptional silencing and CpG methylation induced by siRNAs targeted to the HIV-1 promoter region. *J. RNAi Gene Silencing*, **1**, 66–78.
7. Yamagishi,M., Ishida,T., Miyake,A., Cooper,D.A., Kelleher,A.D., Suzuki,K. and Watanabe,T. (2009) Retroviral delivery of promoter-targeted shRNA induces long-term silencing of HIV-1 transcription. *Microbes. Infect.*, **11**, 500–508.
8. Pollard,T.D. and Cooper,J.A. (2009) Actin, a central player in cell shape and movement. *Science*, **326**, 1208–1212.
9. Hofmann,W.A., Stojiljkovic,L., Fuchsova,B., Vargas,G.M., Mavrommatis,E., Philimonenko,V., Kysela,K., Goodrich,J.A., Lessard,J.L., Hope,T.J. *et al.* (2004) Actin is part of pre-initiation complexes and is necessary for transcription by RNA polymerase II. *Nat. Cell. Biol.*, **6**, 1094–1101.
10. Ishida,T.K., Tojo,T., Aoki,T., Kobayashi,N., Ohishi,T., Watanabe,T., Yamamoto,T. and Inoue,J. (1996) TRAF5, a novel tumor necrosis factor receptor-associated factor family protein, mediates CD40 signaling. *Proc. Natl Acad. Sci. USA*, **93**, 9437–9442.
11. Berg,J., Doe,B., Steimer,K.S. and Wabl,M. (1991) HeLa-LAV, an epithelial cell line stably infected with HIV-1. *J. Virol. Methods*, **34**, 173–180.
12. Abramoff,M.D., Magelhaes,P.J. and Ram,S.J. (2004) Image Processing with ImageJ. *Biophoton. Int.*, **11**, 36–42.
13. Zinchik,V., Zinchuk,O. and Okada,T. (2007) Qualitative colocalization analysis of multicolor confocal immunofluoresence microscopy images: pushing pixels to explore biological phenomena. *Acta Histochem. Cytochem.*, **40**, 101–111.
14. Suzuki,K., Craddock,B.P., Okamoto,N., Kano,T. and Steigbigel,R.T. (1993) Poly A-linked colorimetric microtiter plate assay for HIV reverse transcriptase. *J. Virol. Methods*, **44**, 189–198.
15. Babakov,V.N., Petukhova,O.A., Turoverova,L.V., Kropacheva,I.V., Tentler,D.G., Bolshakova,A.V., Podolskaya,E.P., Magnusson,K.E. and Pinaev,G.P. (2008) RelA/NF-kappaB transcription factor associates with alpha-actinin-4. *Exp. Cell Res.*, **314**, 1030–1038.
16. Kazuo Suzuki,T.I., Yamagishi,M., Ahlenstiel,C., Swaminathan,S., Marks,K., Murray,D., McCartney,E.M., Beard,M.R., Alexander,M., Purcell,D.F.J. *et al.* (2011) Transcriptional gene silencing of HIV-1 through promoter targeted RNA is highly specific. *RNA Biol.*, November 1 (epub ahead of print).
17. Jinek,M. and Doudna,J.A. (2009) A three-dimensional view of the molecular machinery of RNA interference. *Nature*, **457**, 405–412.
18. Jakymiw,A., Lian,S., Eystathioy,T., Li,S., Satoh,M., Hamel,J.C., Fritzler,M.J. and Chan,E.K. (2005) Disruption of GW bodies impairs mammalian RNA interference. *Nat. Cell. Biol.*, **7**, 1267–1274.
19. Janowski,B.A., Huffman,K.E., Schwartz,J.C., Ram,R., Nordsell,R., Shames,D.S., Minna,J.D. and Corey,D.R. (2006) Involvement of AGO1 and AGO2 in mammalian transcriptional silencing. *Nat. Struct. Mol. Biol.*, **13**, 787–792.
20. Liu,J., Carmell,M.A., Rivas,F.V., Marsden,C.G., Thomson,J.M., Song,J.J., Hammond,S.M., Joshua-Tor,L. and Hannon,G.J. (2004) Argonaute2 is the catalytic engine of mammalian RNAi. *Science*, **305**, 1437–1441.
21. Meister,G., Landthaler,M., Patkaniowska,A., Dorsett,Y., Teng,G. and Tuschl,T. (2004) Human Argonaute2 mediates RNA cleavage targeted by miRNAs and siRNAs. *Mol. Cell*, **15**, 185–197.
22. Cameron,P.U., Saleh,S., Sallmann,G., Solomon,A., Wightman,F., Evans,V.A., Boucher,G., Haddad,E.K., Sekaly,R.P., Harman,A.N. *et al.* (2010) Establishment of HIV-1 latency in resting CD4+ T cells depends on chemokine-induced changes in the actin cytoskeleton. *Proc. Natl Acad. Sci. USA*, **107**, 16934–16939.
23. Wulf,E., Deboben,A., Bautz,F.A., Faulstich,H. and Wieland,T. (1979) Fluorescent phallotoxin, a tool for the visualization of cellular actin. *Proc. Natl Acad. Sci. USA*, **76**, 4498–4502.
24. Sampath,P. and Pollard,T.D. (1991) Effects of cytochalasin, phalloidin, and pH on the elongation of actin filaments. *Biochemistry*, **30**, 1973–1980.
25. Makhnevych,T., Lusk,C.P., Anderson,A.M., Aitchison,J.D. and Wozniak,R.W. (2003) Cell cycle regulated transport controlled by alterations in the nuclear pore complex. *Cell*, **115**, 813–823.
26. Weinberg,M.S., Villeneuve,L.M., Ehsani,A., Amarzguioui,M., Aagaard,L., Chen,Z.X., Riggs,A.D., Rossi,J.J. and Morris,K.V. (2006) The antisense strand of small interfering RNAs directs histone methylation and transcriptional gene silencing in human cells. *RNA*, **12**, 256–262.
27. Schwartz,J.C., Younger,S.T., Nguyen,N.B., Hardy,D.B., Monia,B.P., Corey,D.R. and Janowski,B.A. (2008) Antisense transcripts are targets for activating small RNAs. *Nat. Struct. Mol. Biol.*, **15**, 842–848.
28. Aizer,A., Brody,Y., Ler,L.W., Sonenberg,N., Singer,R.H. and Shav-Tal,Y. (2008) The dynamics of mammalian P body transport, assembly, and disassembly in vivo. *Mol. Biol. Cell*, **19**, 4154–4166.
29. Carmichael,J.B., Stoica,C., Parker,H., McCaffery,J.M., Simmonds,A.J. and Hobman,T.C. (2006) RNA interference effector proteins localize to mobile cytoplasmic puncta in Schizosaccharomyces pombe. *Traffic*, **7**, 1032–1044.
30. Sweet,T.J., Boyer,B., Hu,W., Baker,K.E. and Coller,J. (2007) Microtubule disruption stimulates P-body formation. *RNA*, **13**, 493–502.
31. Stoica,C., Park,J., Pare,J.M., Willows,S. and Hobman,T.C. (2010) The Kinesin motor protein Cut7 regulates biogenesis and function of Ago1-complexes. *Traffic*, **11**, 25–36.
32. Pendleton,A., Pope,B., Weeds,A. and Koffer,A. (2003) Latrunculin B or ATP depletion induces cofilin-dependent translocation of actin into nuclei of mast cells. *J. Biol. Chem.*, **278**, 14394–14400.
33. Zhen,Y.Y., Libotte,T., Munck,M., Noegel,A.A. and Korenbaum,E. (2002) NUANCE, a giant protein connecting the nucleus and actin cytoskeleton. *J. Cell. Sci.*, **115**, 3207–3222.
34. Zhang,Q., Ragnauth,C.D., Skepper,J.N., Worth,N.F., Warren,D.T., Roberts,R.G., Weissberg,P.L., Ellis,J.A. and Shanahan,C.M. (2005) Nesprin-2 is a multi-isomeric protein that binds lamin and emerin at the nuclear envelope and forms a subcellular network in skeletal muscle. *J. Cell. Sci.*, **118**, 673–687.
35. Holaska,J.M., Kowalski,A.K. and Wilson,K.L. (2004) Emerin caps the pointed end of actin filaments: evidence for an actin cortical network at the nuclear inner membrane. *PLoS Biol.*, **2**, E231.
36. Kato,M., Sasaki,M., Mizuno,S. and Harata,M. (2001) Novel actin-related proteins in vertebrates: similarities of structure and expression pattern to Arp6 localized on Drosophila heterochromatin. *Gene*, **268**, 133–140.
37. Ohfuchi,E., Kato,M., Sasaki,M., Sugimoto,K., Oma,Y. and Harata,M. (2006) Vertebrate Arp6, a novel nuclear actin-related protein, interacts with heterochromatin protein 1. *Eur. J. Cell Biol.*, **85**, 411–421.

38. Zhao,K., Wang,W., Rando,O.J., Xue,Y., Swiderek,K., Kuo,A. and Crabtree,G.R. (1998) Rapid and phosphoinositol-dependent binding of the SWI/SNF-like BAF complex to chromatin after T lymphocyte receptor signaling. *Cell*, **95**, 625–636.
39. Hock,J., Weinmann,L., Ender,C., Rudel,S., Kremmer,E., Raabe,M., Urlaub,H. and Meister,G. (2007) Proteomic and functional analysis of Argonaute-containing mRNA-protein complexes in human cells. *EMBO Rep.*, **8**, 1052–1060.
40. Weinmann,L., Hock,J., Ivacevic,T., Ohrt,T., Mutze,J., Schwille,P., Kremmer,E., Benes,V., Urlaub,H. and Meister,G. (2009) Importin 8 is a gene silencing factor that targets argonaute proteins to distinct mRNAs. *Cell*, **136**, 496–507.
41. Zhang,S., Kohler,C., Hemmerich,P. and Grosse,F. (2004) Nuclear DNA helicase II (RNA helicase A) binds to an F-actin containing shell that surrounds the nucleolus. *Exp. Cell Res.*, **293**, 248–258.
42. Schindler,M. and Jiang,L.W. (1986) Nuclear actin and myosin as control elements in nucleocytoplasmic transport. *J. Cell Biol.*, **102**, 859–862.
43. Guang,S., Bochner,A.F., Pavelec,D.M., Burkhart,K.B., Harding,S., Lachowiec,J. and Kennedy,S. (2008) An Argonaute transports siRNAs from the cytoplasm to the nucleus. *Science*, **321**, 537–541.
44. Aravin,A.A., Sachidanandam,R., Bourc'his,D., Schaefer,C., Pezic,D., Toth,K.F., Bestor,T. and Hannon,G.J. (2008) A piRNA pathway primed by individual transposons is linked to de novo DNA methylation in mice. *Mol. Cell*, **31**, 785–799.
45. Noto,T., Kurth,H.M., Kataoka,K., Aronica,L., DeSouza,L.V., Siu,K.W., Pearlman,R.E., Gorovsky,M.A. and Mochizuki,K. (2010) The Tetrahymena argonaute-binding protein Giw1p directs a mature argonaute-siRNA complex to the nucleus. *Cell*, **140**, 692–703.